

1960-25

ICTP Conference Graphene Week 2008

25 - 29 August 2008

**Spin-orbit modulated transport in
graphene and nanotubes**

D. Huertas-Hernando

*Norwegian University of Science and Technology
Trondheim
Norway*

F. Guinea

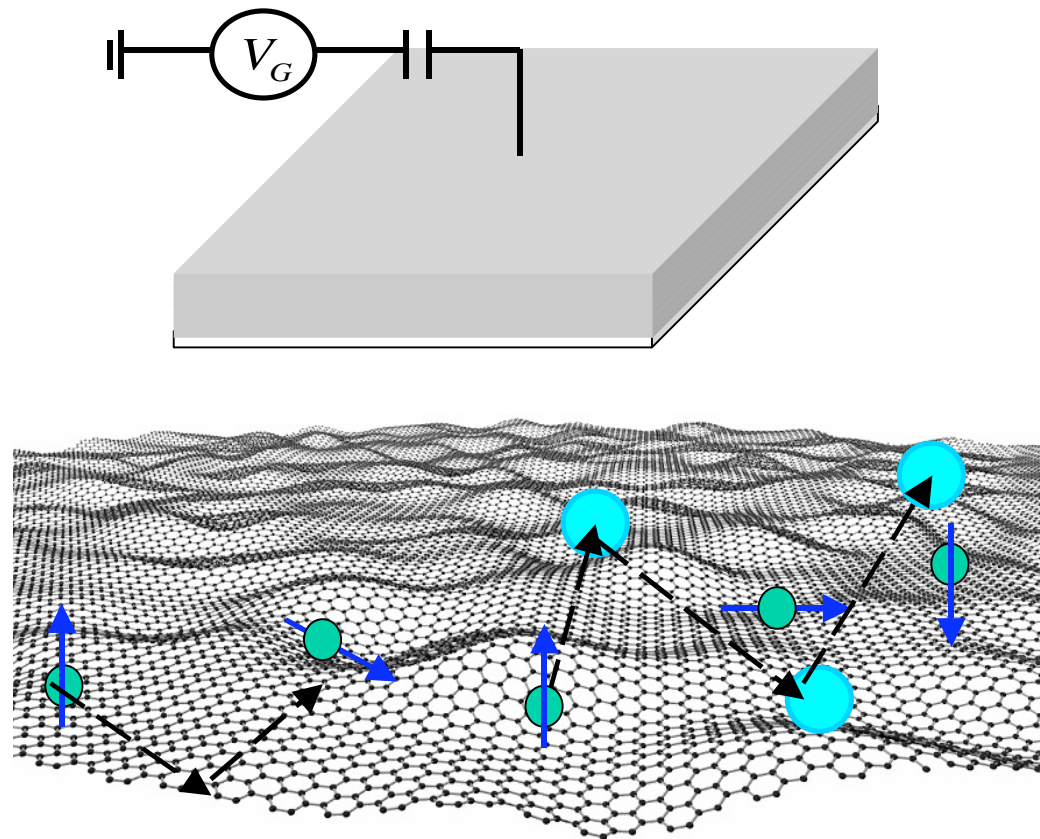
*Consejo Superior de Investigaciones Científicas
Madrid
Spain*

A. Brataas

*Norwegian University of Science and Technology
Trondheim
Norway*

Spin-orbit modulated transport in graphene and nanotubes

D. Huertas-Hernando (NTNU), F. Guinea (CSIC), A. Brataas (NTNU)



Outline

- Spin orbit coupling in graphene
- Spin scattering at boundaries of nanoribbons + so
- Spin precession in nanotubes
- Scattering due to defects+so
 - Weak scatterers
 - Strong scatterers
- Spin relaxation(*):
 - D'yakonov-Perel'
 - Elliot-Yafet

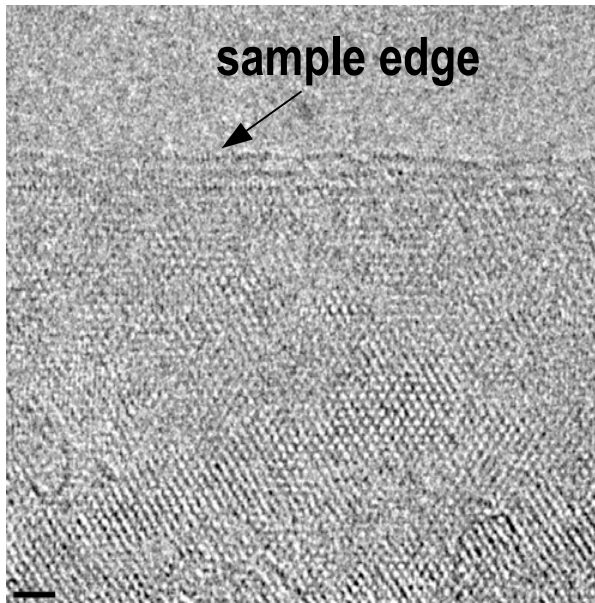
Spin-Orbit Hamiltonian for graphene

$$\mathcal{H}_T = \int d^2\vec{r} \Psi^\dagger \left(-i\hbar v_F [\hat{\sigma}_y \hat{\partial}_x - \hat{\tau}_z \hat{\sigma}_x \hat{\partial}_y] + \Delta_{\text{int}} [\hat{\tau}_z \hat{\sigma}_z \hat{s}_z] + \frac{\Delta_R}{2} [\hat{\sigma}_x \hat{s}_y + \hat{\tau}_z \hat{\sigma}_y \hat{s}_x] \right) \Psi$$

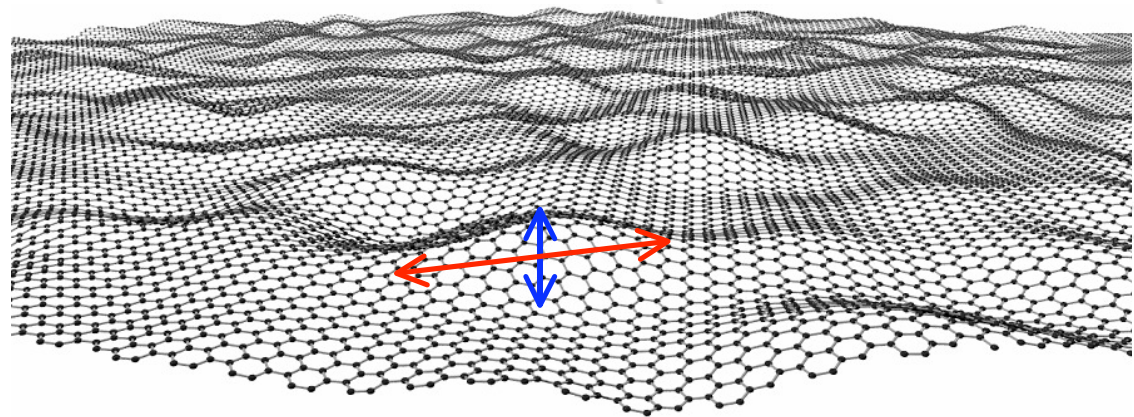
- SO Hamiltonian obtained by Kane & Mele PRL **95**, 226801 (2005).
- $\Delta_R = \Delta_\varepsilon + \Delta_{\text{curv}}$ D. H-H *et al.*, Phys. Rev. B **74**, 155426 (2006).
- H. Min *et al.*, Phys. Rev. B, **74**, 165310 (2006) : $\Delta_R = \Delta_\varepsilon$ but no Δ_{curv} .

Intrinsic Microscopic Crumpling

atomic resolution TEM
ripple contrast appears for >1 layer

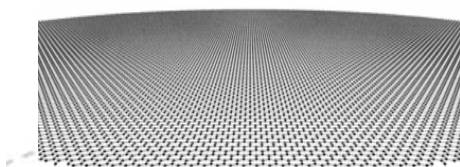


Courtesy of A. Geim&D. Obergfell

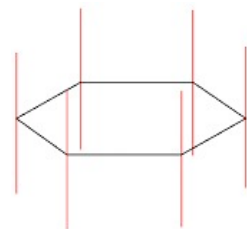


↑ height $\approx 5\text{\AA}$; size $< 5\text{nm}$;
strain $\approx 1\%$

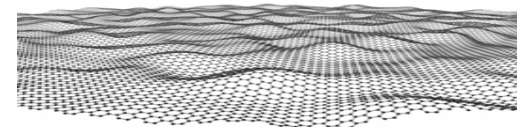
real space



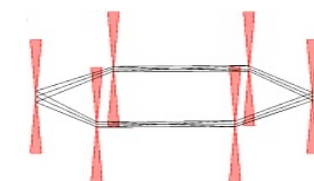
reciprocal space



real space



reciprocal space



Ripples in graphene: Single layer graphene on SiO₂

M. Ishigami, J. H. Chen, W. G. Cullen, M. S. Fuhrer and E. D. Williams, *Nano Letters* **7**, 6 (2007)

E. Stolyarova, K. T. Rim, S. Ryu, J. Maultzsch, P. Kim, L. E. Brus, T. F. Heinz, M. S. Hybertsen and G. W. Flynn, *Proc. Nat. Acad. Sci.* **104**, 9209 (2007)

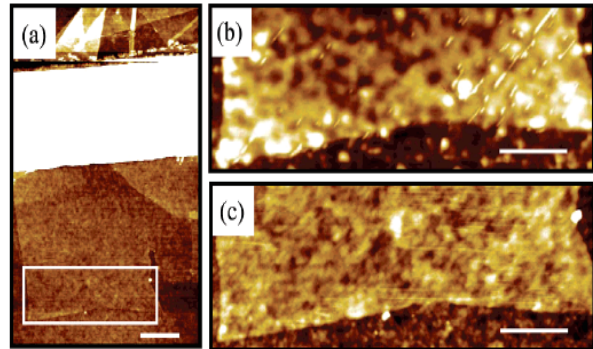


Figure 2. (a) AFM topography of graphene deposited on SiO₂. Thin graphite flakes are generated using the mechanical exfoliation technique¹ on thermally grown SiO₂ with the thickness of 300 nm. Monolayer graphite flakes (graphene) are located using optical and atomic force microscopy.⁹ The e-beam lithography defined electrode,³³ approximately 80 nm in height and 1.5 μ m in width, is the white area nearly horizontal to the image. The black square indicates the region shown in parts b and c of Figure 1. The scale bar is 500 nm. (b) Graphene sheet prior to the cleaning procedure described in text. The scale bar is 300 nm. (c) Graphene sheet after the cleaning procedure. The standard deviation of the height variation in a square of side 600 nm is approximately 3 Å after the treatment compared to 8 Å before the treatment. The scale bar is 300 nm. Images a–c were acquired using intermittent-contact mode AFM in air.

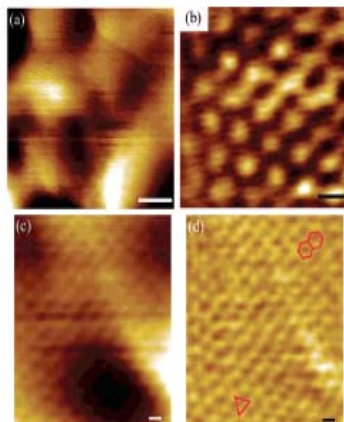
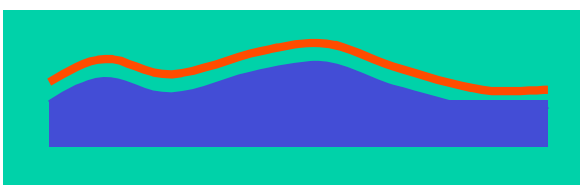


Figure 3. (a) A typical high-pass STM image of the graphene sheet shown in Figure 2a. Peak-to-peak height variation of the image is approximately 2.5 nm. $V_{bias} = 11$ V and $I_{bias} = 0.3$ nA. The scale bar is 2 nm. (b) Atomically resolved image of a graphene sheet. $V_{bias} = 1.0$ V and $I_{bias} = 24$ pA. The scale bar is 2.5 Å. (c) STM image of smooth area. The scale bar is 2.5 Å. $V_{bias} = 1.2$ V and $I_{bias} = 0.35$ nA. (d) A high-pass filtered image of the large area seen above in (a). Both triangular and hexagonal patterns are observed. The orientation of the red triangle and hexagon are same. The scale bar is 2.5 Å.



The graphene layer follows the corrugation of the substrate

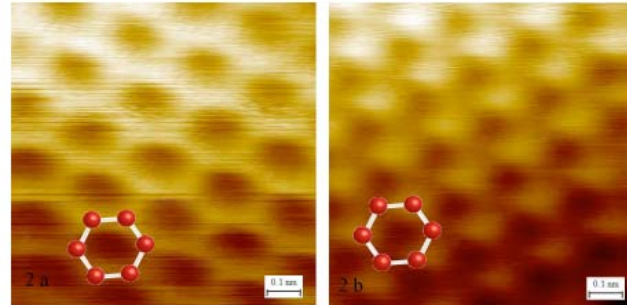


Figure 2. STM topographic images of different regions of the graphene flake of Fig. 1. The images were obtained with $V_{bias} = +1$ V (sample potential), $I = 1$ nA, and a scan area of 1 nm^2 . A model of the underlying atomic structure is shown as a guide to the eye. (a) Image from a single-layer of graphene (region I of Fig. 1). A honeycomb structure is observed. (b) Image of the multi-layer portion of the sample (region II of Fig 1). The characteristic “three-for-six” STM image of the surface of bulk graphite is observed.

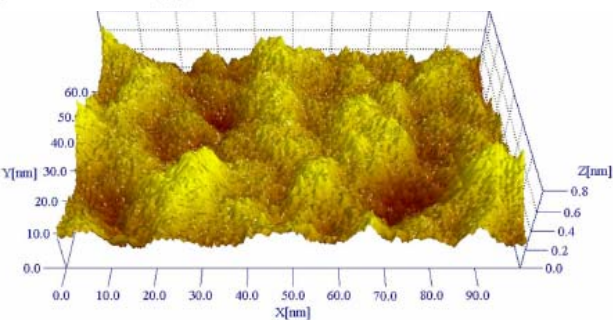


Figure 3. Stereographic plot of a large-scale (100×62 nm) STM image of a single-layer graphene film on the silicon dioxide surface. The STM scanning conditions were: $V_{bias} = 1$ V (sample potential) and $I = 0.6$ nA. The 0.8-nm scale of the vertical (Z) coordinate is greatly enlarged to accentuate the surface features.

Estimates

D. H-H, F. Guinea and A. Brataas, Phys. Rev. B **74**, 155426 (2006)

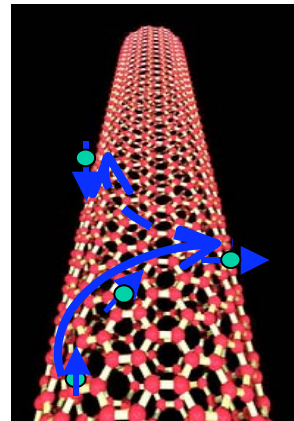
	Kane & Mele
$\frac{3}{4} \frac{\Delta^2}{V_1} \left(\frac{V_1}{V_2} \right)^4$	0.01K
$\frac{2\sqrt{2}}{3} \frac{\Delta \lambda e \mathcal{E}}{V_2}$	0.07K
$\frac{\Delta(V_{pp\sigma} - V_{pp\pi})}{V_1} \left(\frac{a}{R_1} + \frac{a}{R_2} \right) \left(\frac{V_1}{V_2} \right)^2$	0.2K

Kane & Mele
 $\Delta_{\text{int}} \sim 2.4 K(!)$
 $\Delta_{\varepsilon} \sim 2.5 mK(!)$
 $\rightarrow \sim \frac{1.6 meV}{d[nm]}$

$$\begin{aligned} {}^1)\mathcal{E} &\sim 50V/300nm \\ {}^2)R &\sim 50 - 100nm \end{aligned}$$

Nanotubes

T. Ando, JPSJ **69**, 1757 (2000); A. De Martino *et. al.*, PRL **88**, 206402 (2002).
D. H-H *et al.*, PRB **74**, 155426 (2006); D. Bulaev *et al.*, PRB **77**, 235301 (2008).



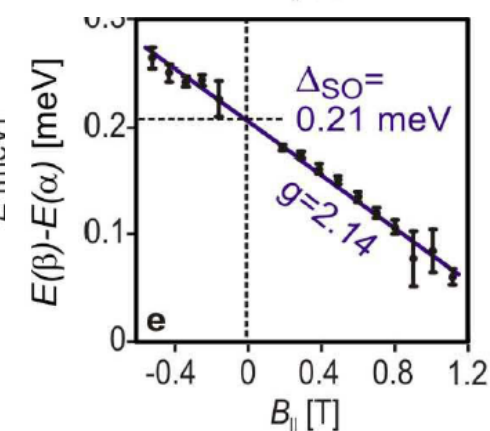
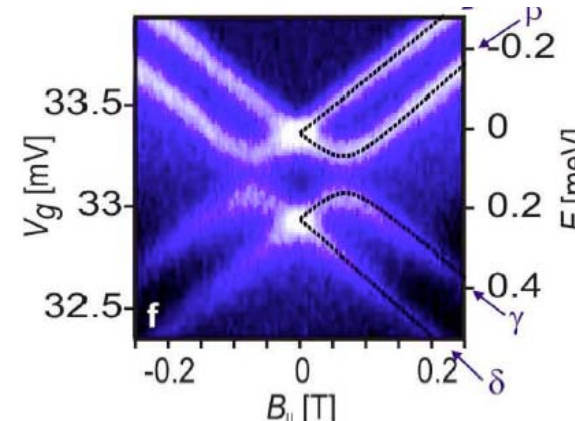
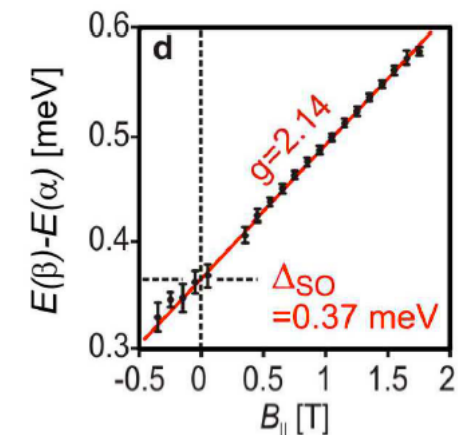
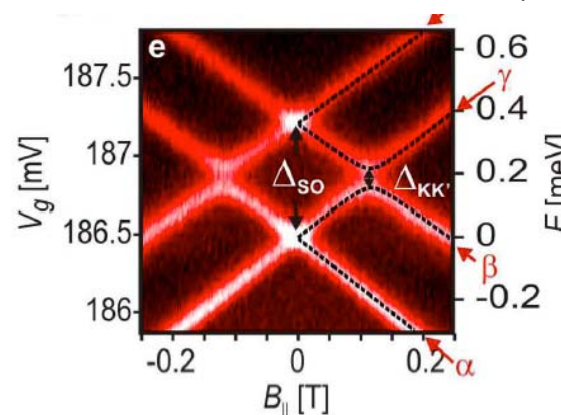
$$\Delta_{so}^{Exp-e} \approx \frac{1.9 \text{ meV}}{d[\text{nm}]}$$

$$\Delta_{so}^{Theory} \approx \frac{1.6 \text{ meV}}{d[\text{nm}]}$$

$$\Delta_{so}^{Exp-h} \approx \frac{1.0 \text{ meV}}{d[\text{nm}]}$$

- Good agreement between Theory and Experiment
- Gate voltage s-o may improve comparison

Cornell group: *Coupling of Spin and Orbital Motion in NT's*
F. Kuemmeth *et. al.*, Nature Physics **452**, 448 (2008)



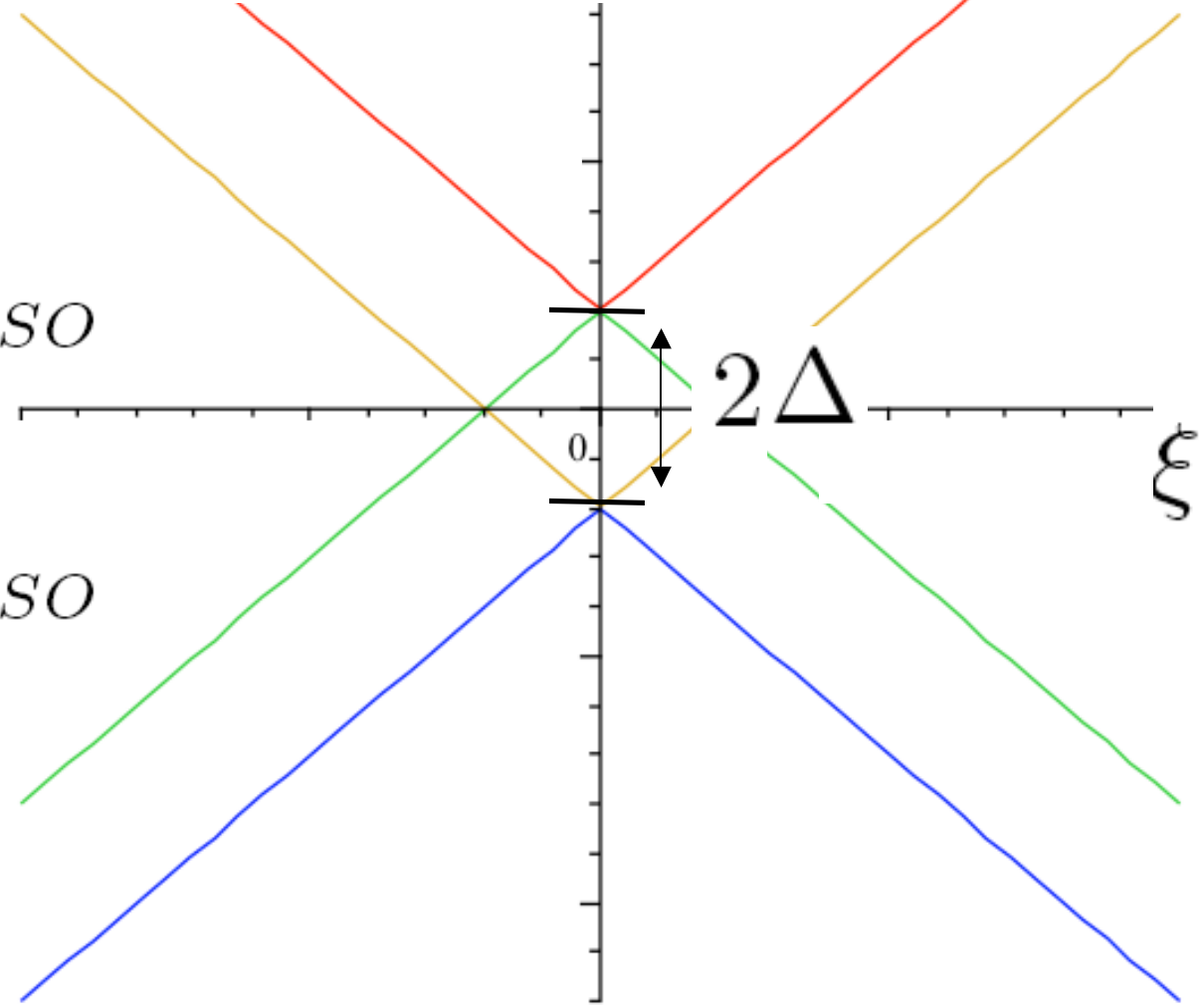
Spin-orbit: Spin & Pseudospin

$$H_K = \hbar v_F k (\vec{n} \cdot \hat{\sigma}) + \Delta_{SO} (\hat{\sigma} \times \hat{\mathbf{s}})_z$$

$$\hbar v_F |\vec{k}| \gg \Delta_{SO}$$

$$\epsilon_{\pm} \approx \hbar v_F |\vec{k}| \pm \Delta_{SO}$$

$$\epsilon_{\pm} \approx \hbar v_F |\vec{k}| \pm \Delta_{SO}$$

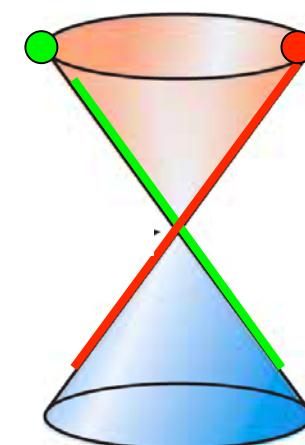
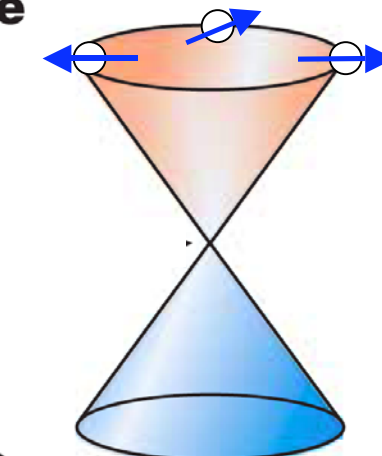


Spin-orbit: Spin & Pseudospin

$$\hbar v_F |\vec{k}| \gg \Delta_{SO}$$

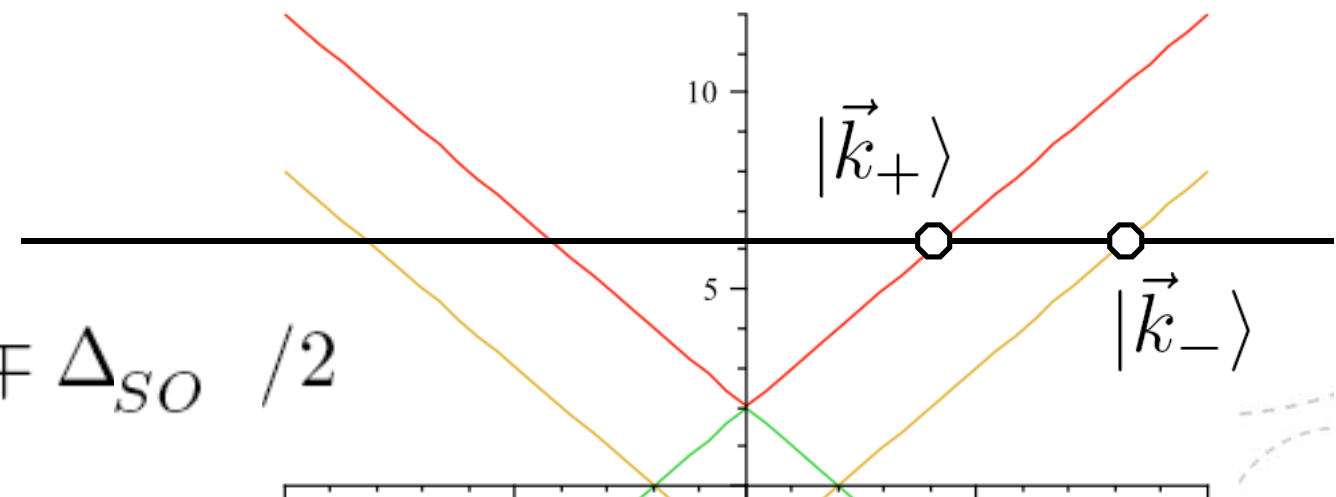
$$|\Psi_{\pm}\rangle \equiv \left[\begin{pmatrix} 1 \\ e^{i\theta} \end{pmatrix} | \uparrow \rangle \pm \begin{pmatrix} e^{i\theta} \\ e^{2i\theta} \end{pmatrix} | \downarrow \rangle \right]$$

$$\equiv \left[\begin{pmatrix} 1 \\ e^{i\theta} \end{pmatrix} \psi_{A,K} \otimes \begin{pmatrix} 1 \\ \pm e^{i\theta} \end{pmatrix} | \uparrow \rangle | \downarrow \rangle \right]$$


 \otimes


Spin-orbit: Spin & Pseudospin

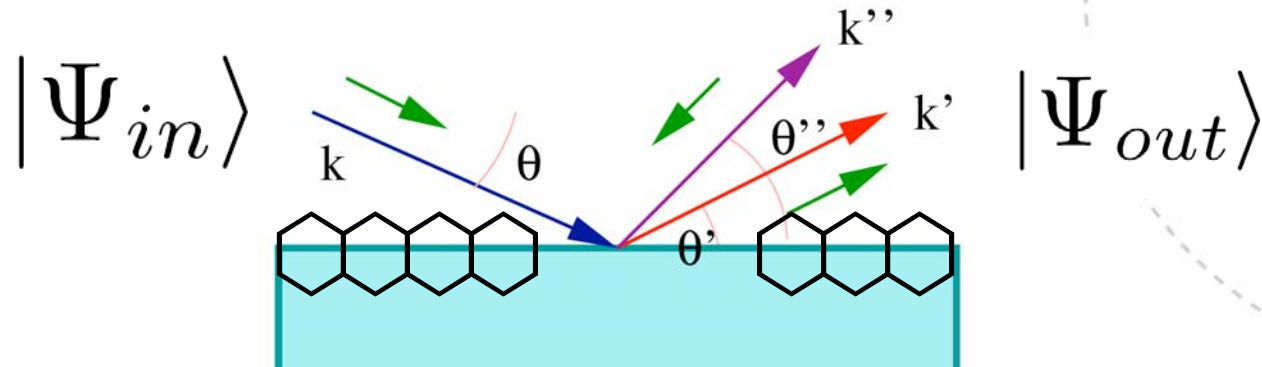
$$\hbar v_F |\vec{k}_\pm| = \epsilon \mp \Delta_{SO} / 2$$



$$|\Psi_{in}\rangle = \cos(\theta/2)|\vec{k}_+\rangle + \sin(\theta/2)|\vec{k}_-\rangle$$

$$\Delta\theta = (k_+ - k_-)L = (\Delta_{SO} \times L) / (\hbar v_F)$$

Spin scattering at (zig-zag_{*})boundaries



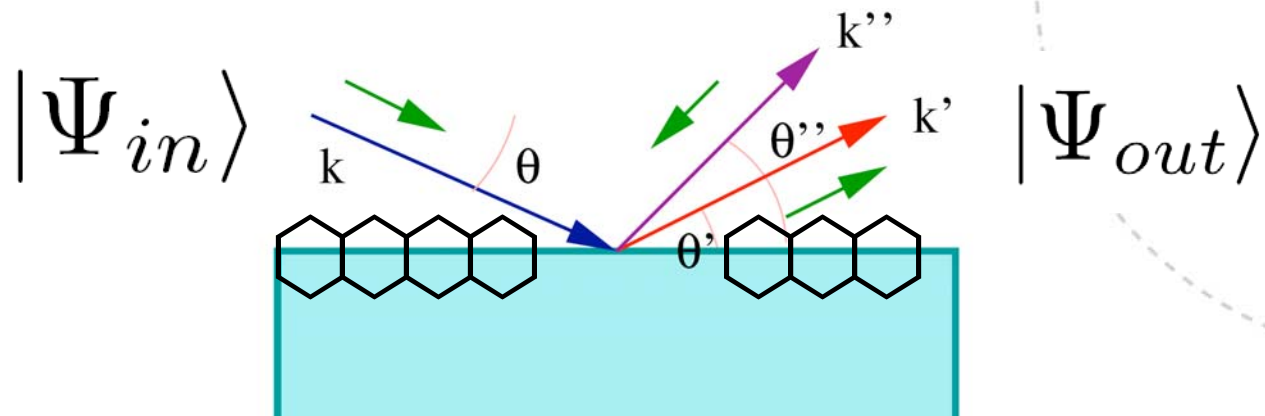
$$\begin{aligned}
 |\Psi_{out}\rangle &\equiv r_1 \left[\begin{pmatrix} 1 \\ e^{i\theta'} \end{pmatrix} |\uparrow\rangle + \begin{pmatrix} e^{i\theta'} \\ e^{2i\theta'} \end{pmatrix} |\downarrow\rangle \right] e^{i\vec{k}' \cdot \vec{r}} + \\
 &+ r_2 \left[\begin{pmatrix} 1 \\ e^{i\theta''} \end{pmatrix} |\uparrow\rangle - \begin{pmatrix} e^{i\theta''} \\ e^{2i\theta''} \end{pmatrix} |\downarrow\rangle \right] e^{i\vec{k}'' \cdot \vec{r}}
 \end{aligned}$$

$$1 + r_1 + r_2 = 0$$

$$e^{i\theta} + r_1 e^{i\theta'} - r_2 e^{i\theta''} = 0$$

*A. R. Akhmerov, C. W. J. Beenakker, PRB 77, 085423 (2008)

Spin scattering at (zig-zag)boundaries



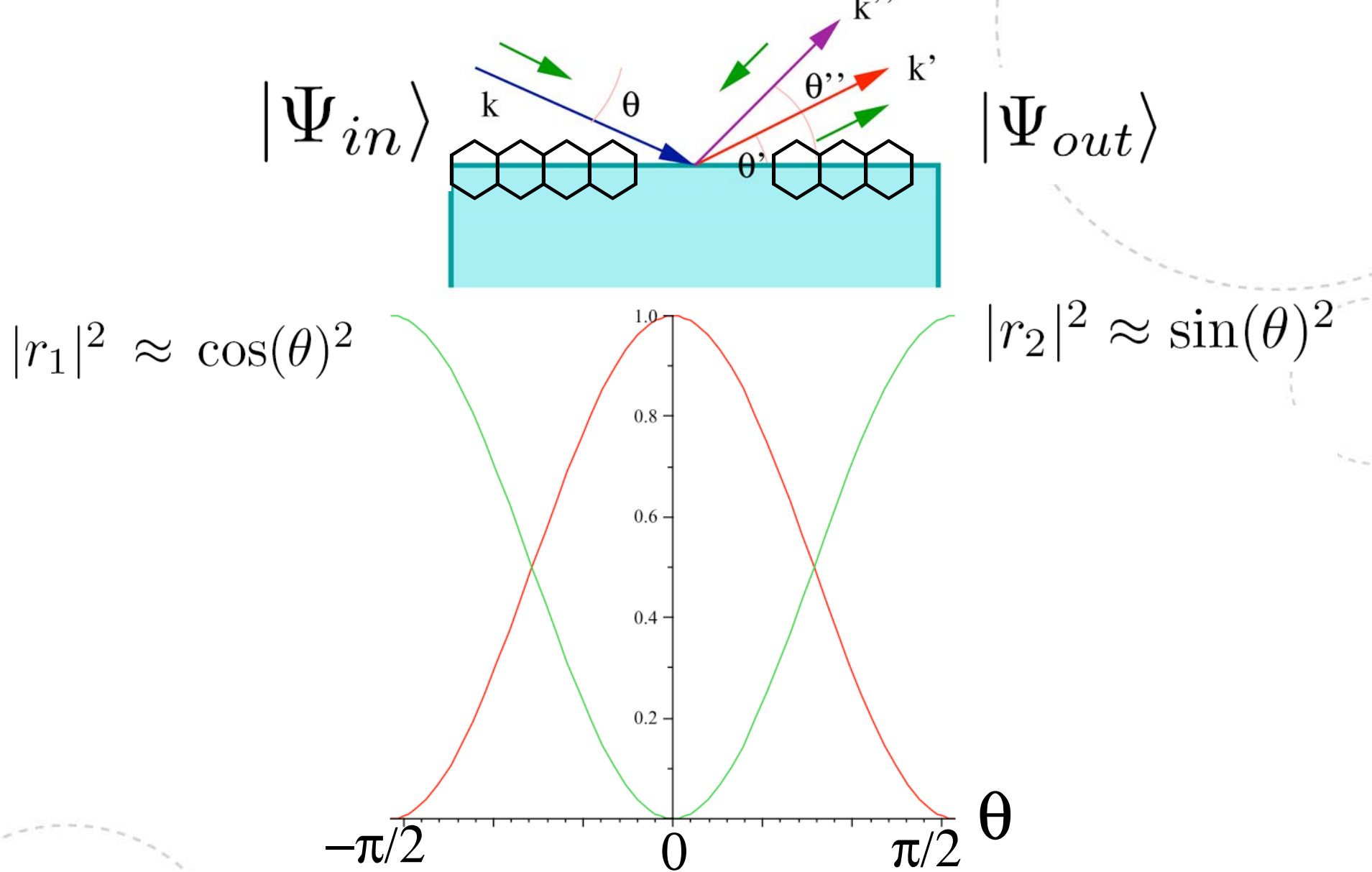
$$|\vec{k}| \cos(\theta) = |\vec{k}''| \cos(\theta'')$$

$$\hbar v_F |\vec{k}| + \frac{\Delta_{SO}}{2} = \hbar v_F |\vec{k}''| - \frac{\Delta_{SO}}{2}$$

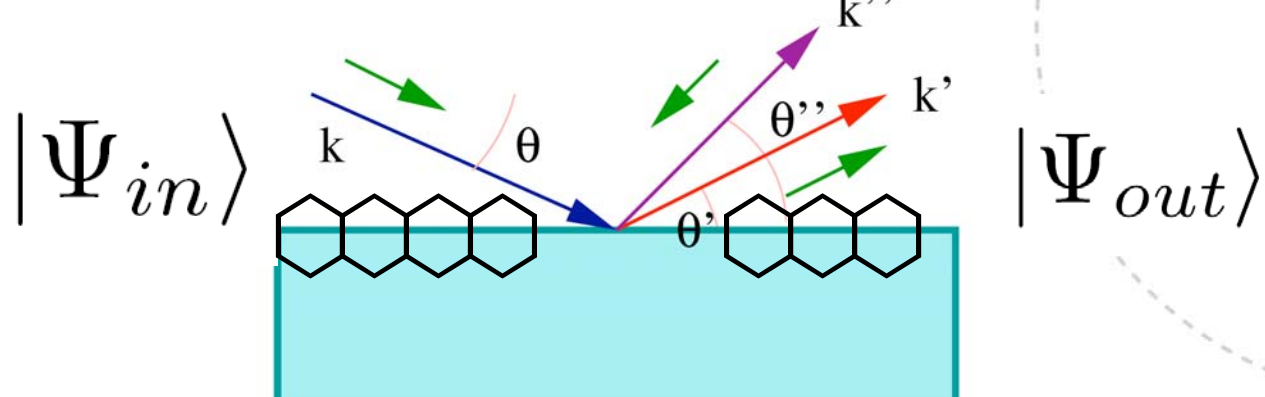
$$r_1 = -\frac{e^{i\theta''} + e^{i\theta}}{e^{i\theta''} + e^{-i\theta}}$$

$$r_2 = -\frac{2i \sin(\theta)}{e^{i\theta''} + e^{-i\theta}}$$

Spin scattering at (zig-zag)boundaries



Spin scattering at (zig-zag)boundaries



$$r_1 = -\frac{e^{i\theta''} + e^{i\theta}}{e^{i\theta''} + e^{-i\theta}}$$

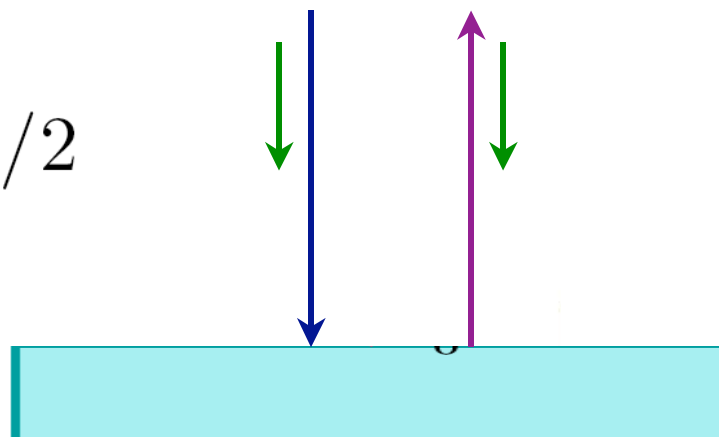
$$|r_1|^2 \approx \cos(\theta)^2$$

$$r_2 = -\frac{2i \sin(\theta)}{e^{i\theta''} + e^{-i\theta}}$$

$$|r_2|^2 \approx \sin(\theta)^2$$

$$\theta = \pi/2 \text{ and } \theta'' = -\pi/2$$

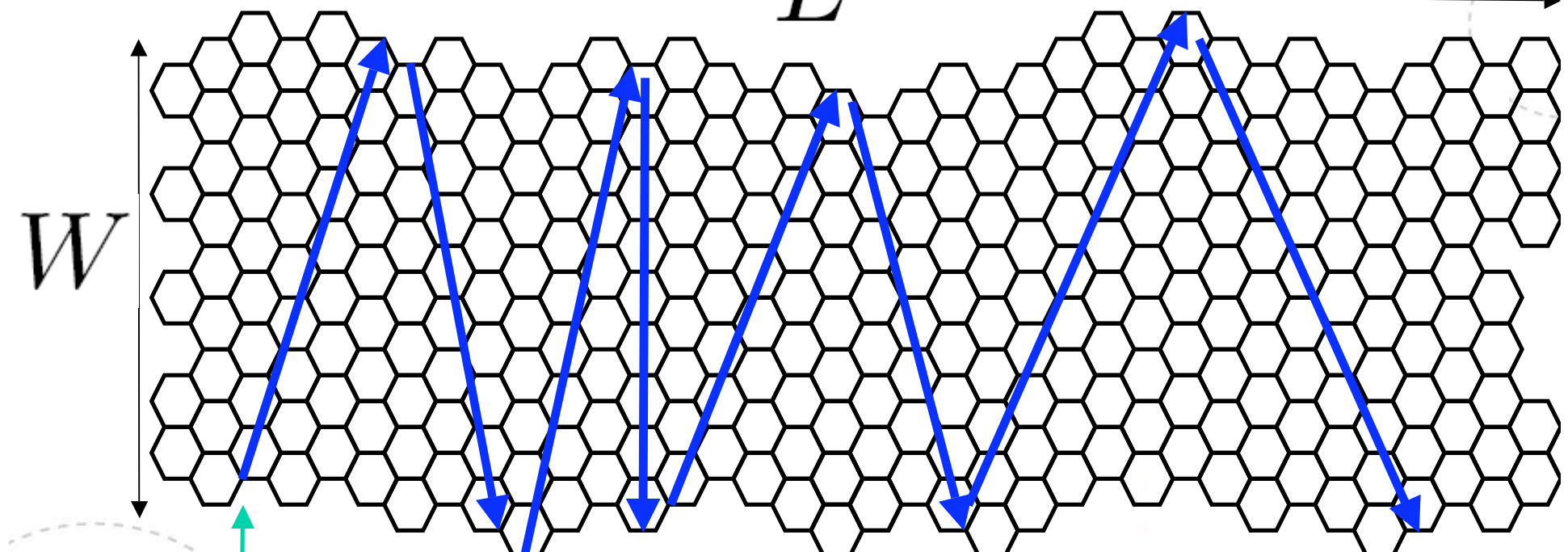
$$r_1 = 0 \text{ and } |r_2| = 1$$



Spin scattering at boundaries

$$\Delta\theta_{\pm} = (\Delta k / |\vec{k}|) \cot(\theta) = (\Delta_{SO} / (\hbar v_F) |\vec{k}|) \cot(\theta)$$

$$L^* \sim 2\pi(\hbar v_F) / \Delta_{SO} \quad L \gtrsim \sqrt{L^* W / 2}$$



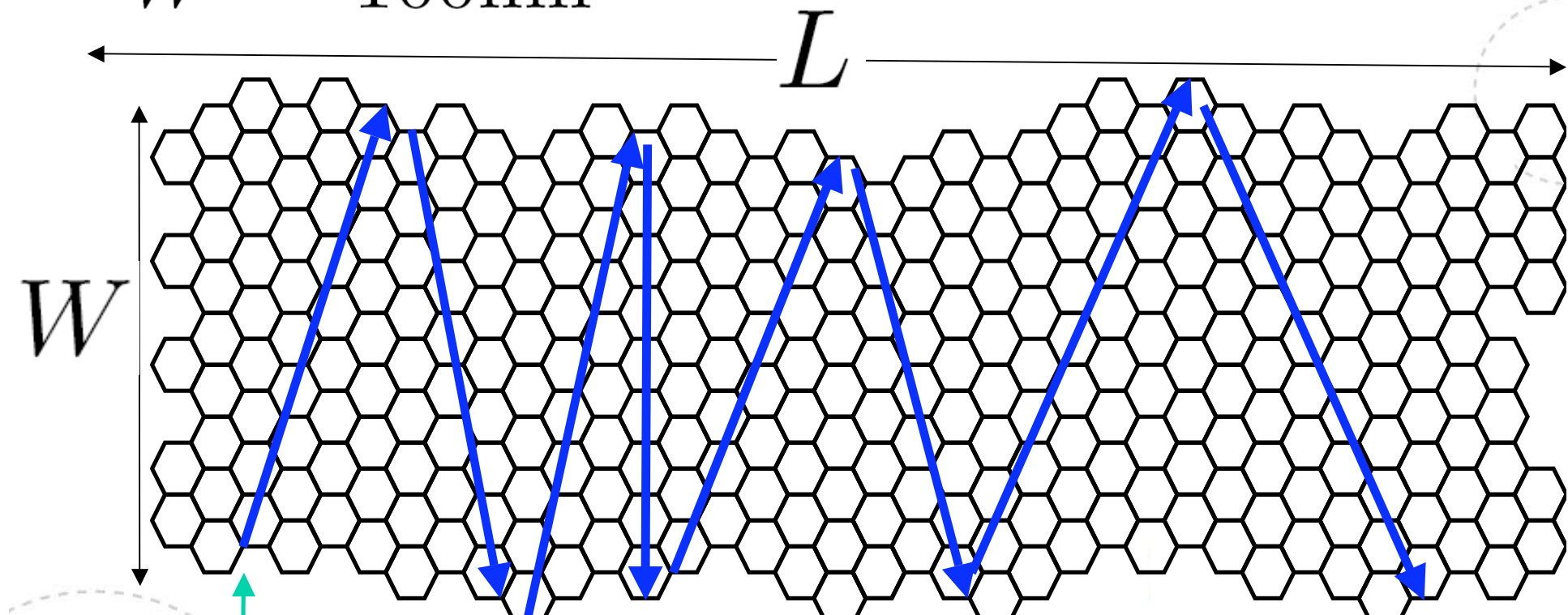
Spin scattering at boundaries

$$L^* \sim 2\pi(\hbar v_F)/\Delta_{SO} \quad L \gtrsim \sqrt{L^* W/2}$$

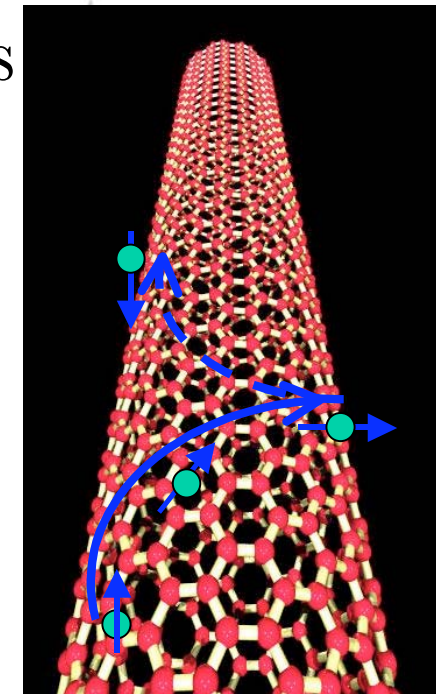
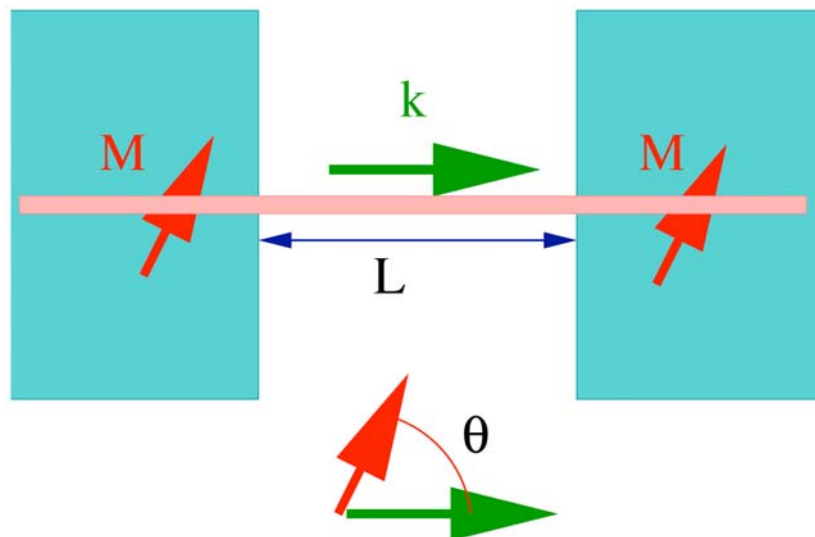
$$\Delta_{\mathcal{E}} \sim 10^{-5} \text{ eV}$$

$$W \sim 100 \text{ nm}$$

$$L \sim 4 \mu\text{m}$$



Spin precession in nanotubes



$$\Delta\theta = (k_+ - k_-)L = (\Delta_{curv} L)/(\hbar v_F)$$

For normal reflection $r_1 = 0$ and $|r_2| = 1$

$$\Delta\theta_n = [\Delta_{curv} L(2n + 1)]/(\hbar v_F)$$

Spin precession in nanotubes

$$\Delta\theta_n = [\Delta_{curv} L(2n + 1)]/(\hbar v_F)$$

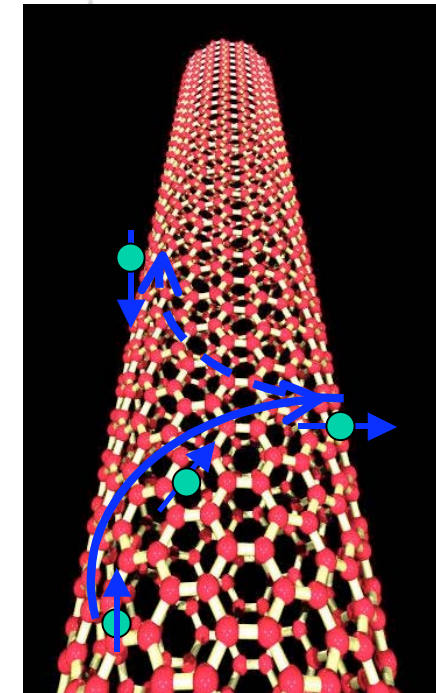
\bar{n} : average number of reflections

$$L(2\bar{n} + 1) \gtrsim L^* = \frac{\hbar v_F}{\Delta_{curv}} 2\pi$$

$$R = 30\text{nm} \rightarrow L^* \approx 150\mu\text{m}$$

$$L = 1\mu\text{m} \rightarrow \bar{n} \sim 10^2$$

$$R \sim \bar{n}h/e^2 \gg h/e^2$$



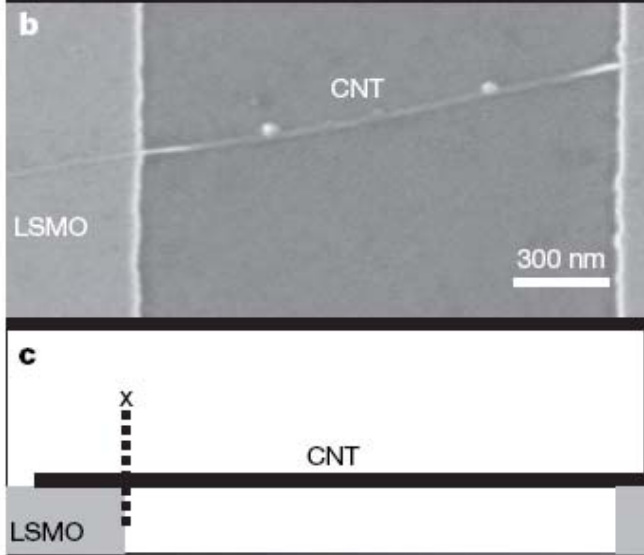
Spin precession in nanotubes

$$R \sim \bar{n}h/e^2 \gg h/e^2$$

NATURE | Vol 445 | 25 January 2007

Transformation of spin information into large electrical signals using carbon nanotubes

Luis E. Hueso¹†, José M. Pruneda^{2,3}†, Valeria Ferrari⁴†, Gavin Burnell¹†, José P. Valdés-Herrera^{1,5}, Benjamin D. Simons⁴, Peter B. Littlewood⁴, Emilio Artacho², Albert Fert⁶ & Neil D. Mathur¹

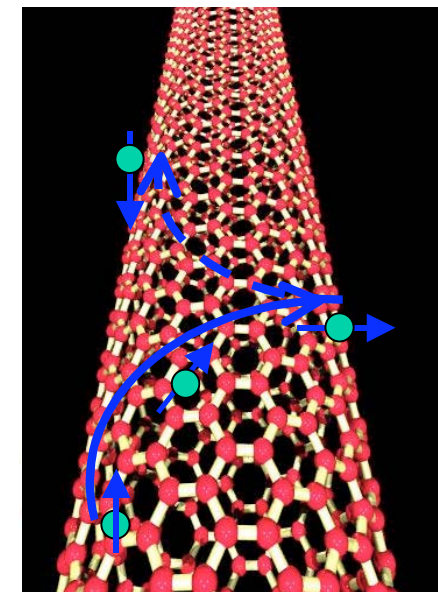


$$l_{sf} = \sqrt{v_F \tau_{sf} \lambda} \approx 50 \mu\text{m}$$

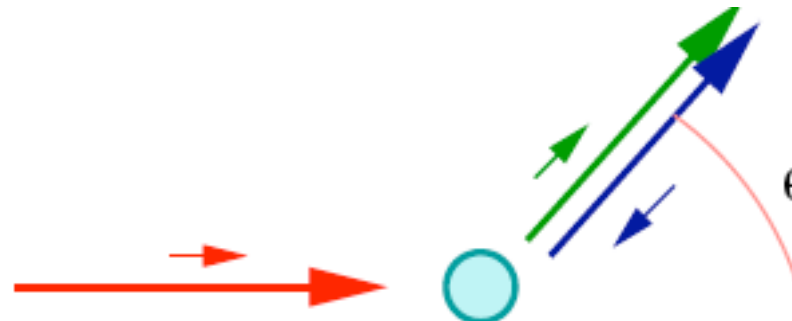
$$\lambda \approx 100 \text{ nm}$$

$$V/I = 10-100 \text{ M}\Omega$$

$$L^* \approx 150 \mu\text{m}$$



Weak scatterers



Born approximation

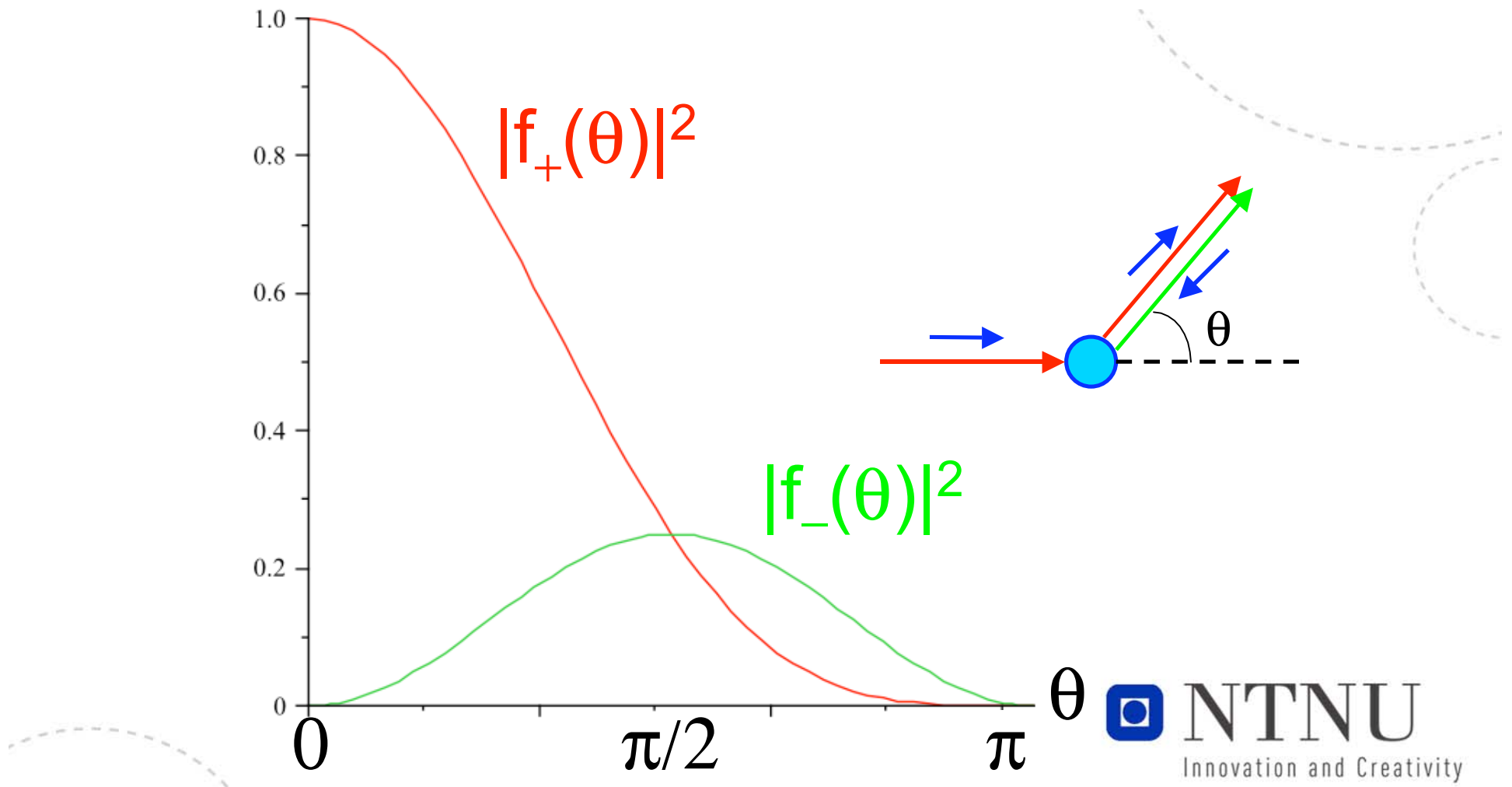
$$\langle \vec{k} | V | \vec{k}' \rangle f_{\pm}(\bar{\theta}) = \int V(r) e^{i(\vec{k} - \vec{k}') \cdot \vec{r}} d^2 \vec{r} f_{\pm}(\bar{\theta})$$

$$f_{\pm}(\bar{\theta}) = \left(1 + e^{i\bar{\theta}}\right) \left(1 \pm e^{i\bar{\theta}}\right) / 4$$

$$\bar{\theta} = \theta_{in} - \theta_{out}$$

Weak scatterers

$$|f_{\pm}(\theta)|^2 = \cos^2\left(\frac{\theta}{2}\right) \times \begin{cases} \cos^2\left(\frac{\theta}{2}\right) & \text{parallel} \\ \sin^2\left(\frac{\theta}{2}\right) & \text{antiparallel} \end{cases}$$

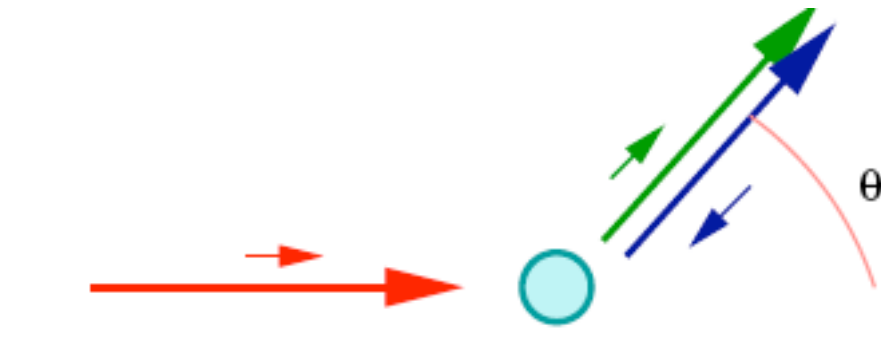


Strong Scatterers: vacancies, adatoms

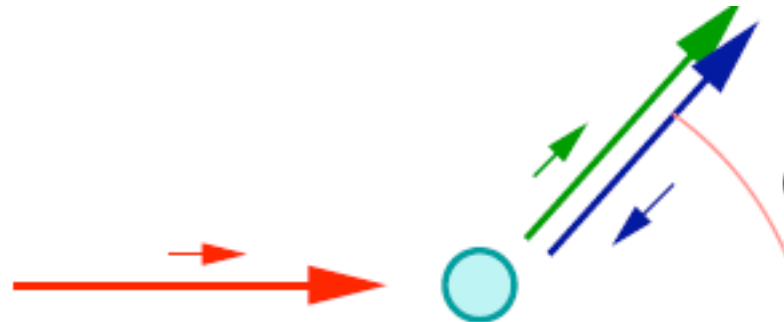
M. Hentschel, F. Guinea, PRB **76**, 1105407 (2007)

$$|\Psi\rangle \equiv \begin{pmatrix} J_{n+1}(kr)e^{i(n+1)\theta} \\ J_n(kr)e^{in\theta} \end{pmatrix} |\uparrow\rangle + \\ + \begin{pmatrix} J_{n+2}(kr)e^{i(n+2)\theta} \\ J_{n+1}(kr)e^{i(n+1)\theta} \end{pmatrix} |\downarrow\rangle$$

$$|\Psi_{out}\rangle \equiv r_1 \left[\begin{pmatrix} Y_{n+1}(kr)e^{i(n+1)\theta} \\ Y_n(kr)e^{in\theta} \end{pmatrix} |\uparrow\rangle + \right. \\ \left. + \begin{pmatrix} Y_{n+2}(kr)e^{i(n+2)\theta} \\ Y_{n+1}(kr)e^{i(n+1)\theta} \end{pmatrix} |\downarrow\rangle \right] + \\ + r_2 \left[\begin{pmatrix} Y_{n+1}(k'r)e^{i(n+1)\theta} \\ Y_n(k'r)e^{in\theta} \end{pmatrix} |\uparrow\rangle - \right. \\ \left. - \begin{pmatrix} Y_{n+2}(k'r)e^{i(n+2)\theta} \\ Y_{n+1}(k'r)e^{i(n+1)\theta} \end{pmatrix} |\downarrow\rangle \right]$$



Strong Scatterers: vacancies, adatoms



$$J_n(kR) + r_1 Y_n(kR) + r_2 Y_n(k'R) = 0$$

$$J_{n+1}(kR) + r_1 Y_{n+1}(kR) - r_2 Y_{n+1}(k'R) = 0$$

$$r_1 = -\frac{J_n(kR)Y_{n+1}(k'R) - J_{n+1}(kR)Y_n(k'R)}{Y_n(kR)Y_{n+1}(k'R) + Y_n(k'R)Y_{n+1}(kR)}$$

$$r_2 = -\frac{J_n(kR)Y_{n+1}(kR) + J_{n+1}(kR)Y_n(kR)}{Y_n(kR)Y_{n+1}(k'R) + Y_n(k'R)Y_{n+1}(kR)}$$

D'yakonov-Perel'

$$H_{SO} = \Delta(\hat{\sigma} \times \hat{e}_z) \cdot \hat{\mathbf{s}} \quad \vec{B}(\sigma) = \Delta(\hat{\sigma} \times \hat{e}_z)$$

D'YAKONOV-PEREL'



$$1/\tau_{s,ii} = \gamma_l^{-1} \tau_p (\overline{\Omega^2} - \overline{\Omega_i^2})$$

$$\tau_{s,ii} \sim \frac{1}{\tau_p} \left(\frac{\hbar}{\Delta} \right)^2$$

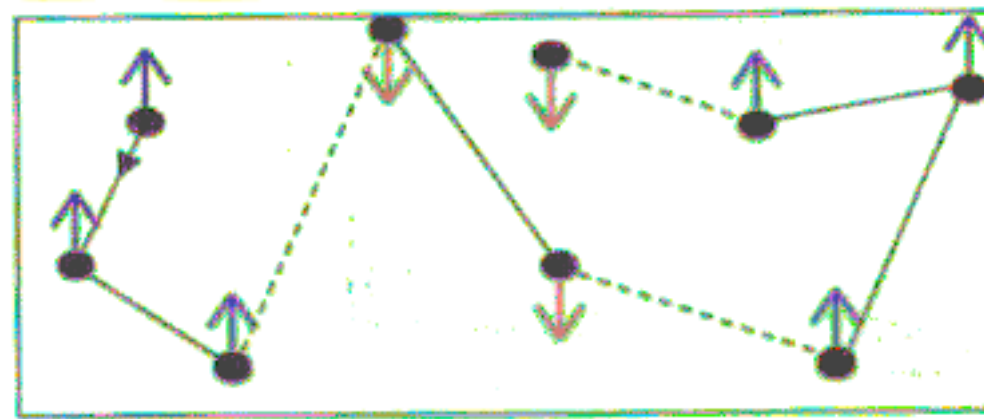
Poster by S. Konschuh et. al.

$$1/\tau_{s,\parallel} = 1/2 \tau_{s,\perp}$$

I. Zutic, J. Fabian, S. Das Sarma
Rev. Mod. Phys. **76**, 323 (2004)

Elliott-Yafet

ELLIOTT-YAFET



$$\Psi_{\mathbf{k}n\uparrow}(\mathbf{r}) = [a_{\mathbf{k}n}(\mathbf{r})|\uparrow\rangle + b_{\mathbf{k}n}(\mathbf{r})|\downarrow\rangle]e^{i\mathbf{k}\cdot\mathbf{r}},$$

$$\Psi_{\mathbf{k}n\downarrow}(\mathbf{r}) = [a_{-\mathbf{k}n}^*(\mathbf{r})|\downarrow\rangle - b_{-\mathbf{k}n}^*(\mathbf{r})|\uparrow\rangle]e^{i\mathbf{k}\cdot\mathbf{r}}$$

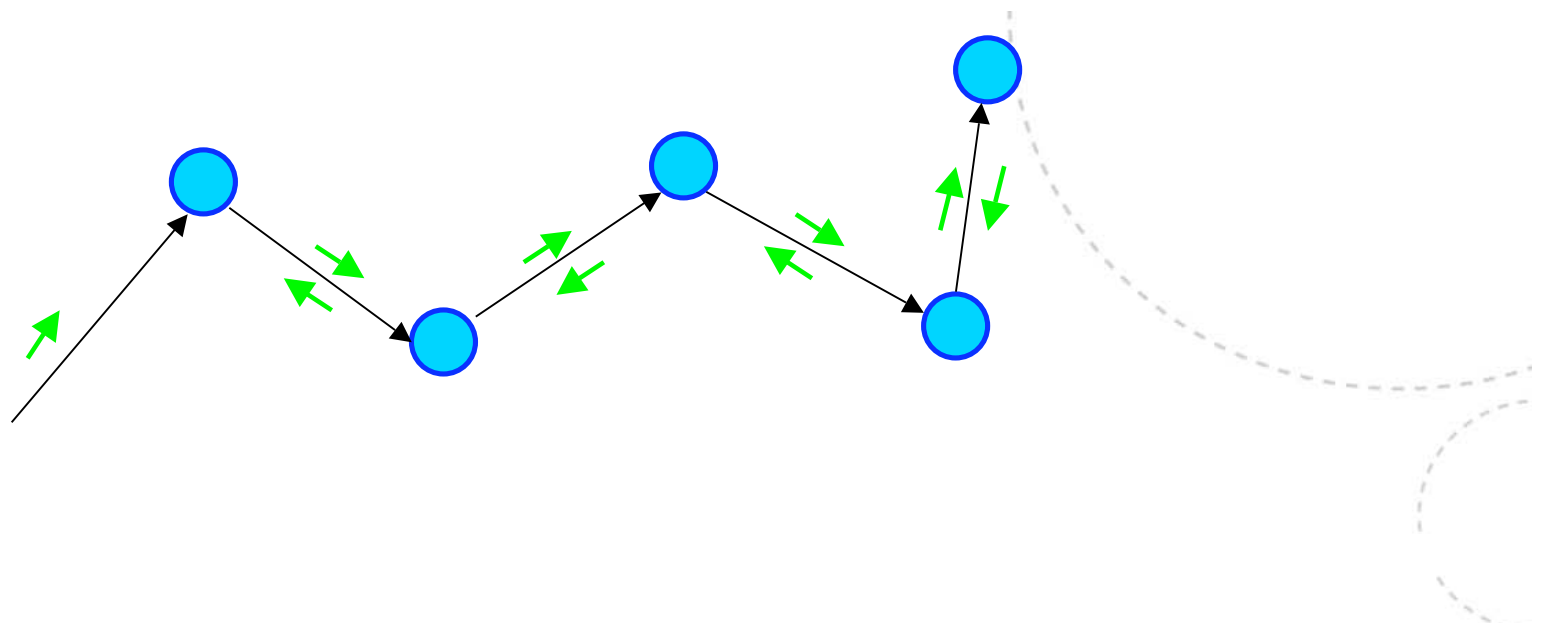
$$1/\tau_s \approx \langle b^2 \rangle / \tau_p \quad |b| \approx \lambda_{so} / \Delta E \ll 1$$

I. Zutic, J. Fabian, S. Das Sarma
 Rev. Mod. Phys. **76**, 323 (2004)



Innovation and Creativity

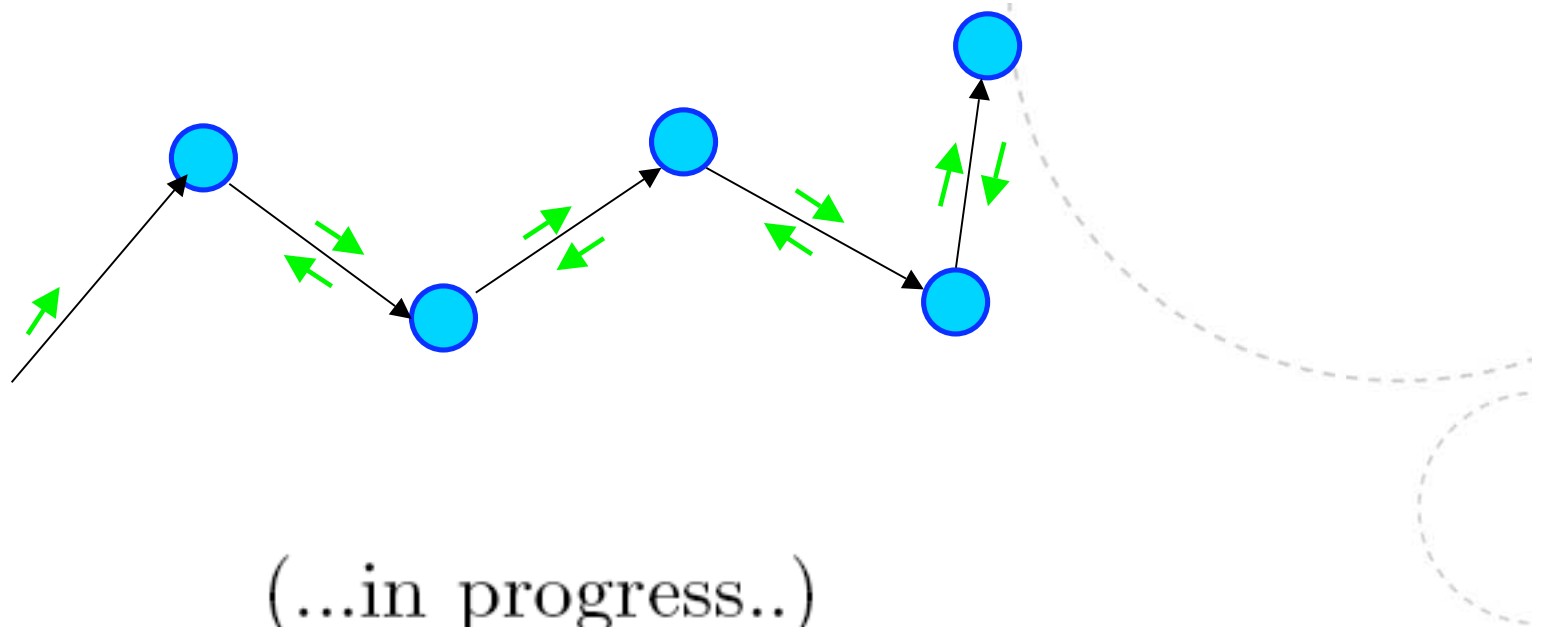
Elliot-Yafet in graphene



$$|\Psi_{in}\rangle \equiv \left[\begin{pmatrix} 1 \\ e^{i\theta} \end{pmatrix} |\uparrow\rangle \pm \begin{pmatrix} e^{i\theta} \\ e^{2i\theta} \end{pmatrix} |\downarrow\rangle \right] e^{i\vec{k}\cdot\vec{r}}$$

$$1/\tau_s \approx \langle ? \rangle / \tau_p$$

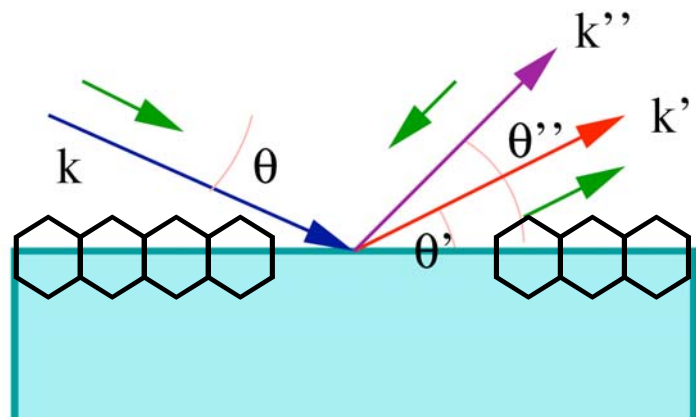
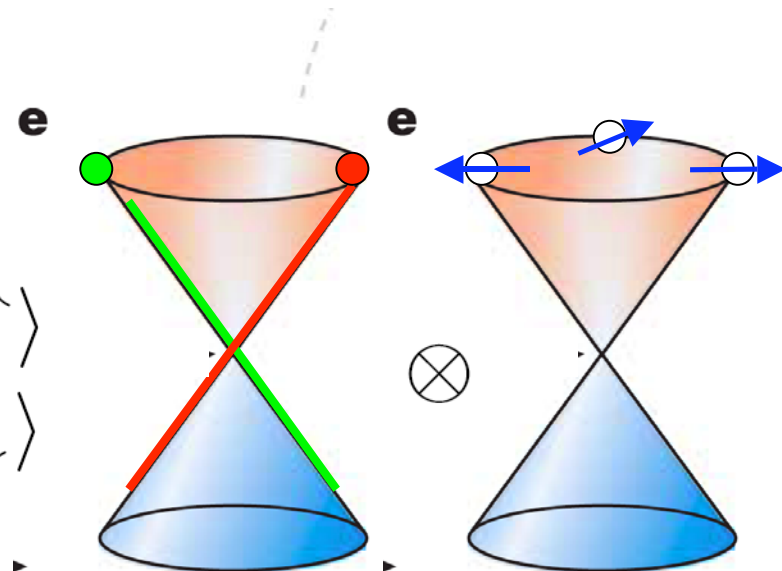
Elliot-Yafet in graphene



$$1/\tau_s \sim <\alpha(r_1, r_2)>/\tau_p$$

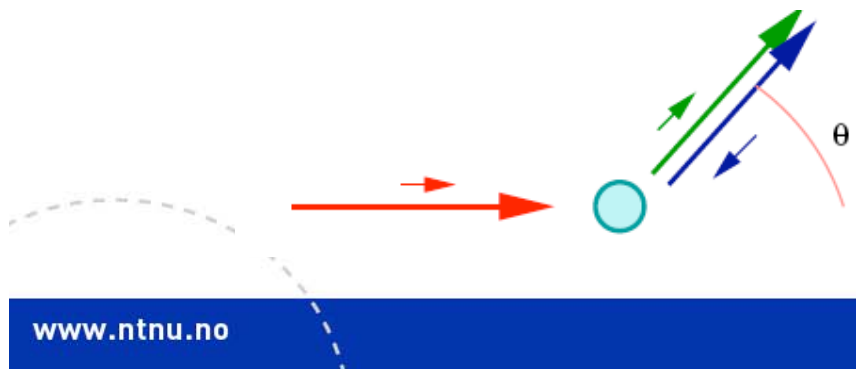
Conclusions

$$\begin{pmatrix} 1 \\ e^{i\theta} \end{pmatrix} \psi_{A,K} \otimes \begin{pmatrix} 1 \\ \pm e^{i\theta} \end{pmatrix} \left| \begin{array}{c} \uparrow \\ \downarrow \end{array} \right\rangle$$



$$|r_2|^2 \approx \sin(\theta)^2$$

$$|r_1|^2 \approx \cos(\theta)^2$$



$$r_1 = -\frac{J_n(kR)Y_{n+1}(k'R) - J_{n+1}(kR)Y_n(k'R)}{Y_n(kR)Y_{n+1}(k'R) + Y_n(k'R)Y_{n+1}(kR)}$$

$$r_2 = -\frac{J_n(kR)Y_{n+1}(kR) + J_{n+1}(kR)Y_n(kR)}{Y_n(kR)Y_{n+1}(k'R) + Y_n(k'R)Y_{n+1}(kR)}$$